Journal of Structural Geology 30 (2008) 1086–1094

Contents lists available at ScienceDirect

Journal of Structural Geology

journal homepage: www.elsevier.com/locate/jsg

Thin pseudotachylytes in faults of the Mt. Abbot quadrangle, Sierra Nevada: Physical constraints for small seismic slip events

W. Ashley Griffith [a,*], Giulio Di Toro [b,c], Giorgio Pennacchioni [b], David D. Pollard [a]

[a] Department of Geological and Environmental Sciences, Stanford University, Stanford, CA 94305, USA
[b] Dipartimento di Geoscienze, Università di Padova, Padova, Italy
[c] Istituto di Geoscienze e Georisorse, Unità operativa di Padova, CNR, Padova, Italy

ARTICLE INFO

Article history:
Received 25 November 2007
Received in revised form 22 April 2008
Accepted 5 May 2008
Available online 15 May 2008

Keywords:
Pseudotachylyte
Faults and faulting
Rupture
Sierra Nevada batholith

ABSTRACT

We document the occurrence of pseudotachylyte (solidified melt produced during seismic slip) along strike-slip faults in the Lake Edison granodiorite of the Mt. Abbot quadrangle, Sierra Nevada, California and provide constraints on ambient conditions during seismic faulting. The pseudotachylytes are less than 0.3 mm thick and are found in faults typically up to 1 cm in thickness. Total measured left-lateral offset along sampled faults is approximately 20 cm. Field and microstructural evidence indicate that the faults exploited pre-existing mineralized joints and show the following overprinting structures (with inferred ambient temperatures): mylonites are more or less coeval with quartz veins (>400 °C), cataclasites and pseudotachylytes (~250 °C) more or less coeval with epidote veins, and zeolite veins (<200 °C). Based on observations of the microstructural textures of faults combined with theoretical heat transfer and energy budget calculations, we suggest that only a fraction (<30%) of the total offset was associated with seismic slip (i.e. pseudotachylyte). The presence of pseudotachylyte in sub-millimeter thick zones lends support for the concept of extreme shear localization during seismic slip. The elusive nature of these pseudotachylytes demonstrates that observations in outcrop and optical microscope are not sufficient to rule out frictional melting as a consequence of seismic slip in similar fault rocks.

1. Introduction

Faults within the Bear Creek drainage of the Mt. Abbot Quadrangle, Sierra Nevada, California (Fig. 1) have received considerable attention during the past two decades as a natural laboratory for investigations of fault mechanics and the evolution of fault architecture in granitic rocks. Most work on the Bear Creek faults has focused on explaining the outcrop-scale fault structure based on continuum and fracture mechanics models (e.g. Segall and Pollard, 1983b; Martel and Pollard, 1989; Bürgmann and Pollard, 1994; d'Alessio and Martel, 2004). Recently these faults have been included in studies of short term dynamic (i.e. coseismic) mechanisms operating near the base of the seismogenic zone (e.g. Shipton et al., 2006a,b). However, evidence that seismic slip occurred along these faults (i.e. the presence of pseudotachylytes: Cowan, 1999) has not been documented.

This paper reports the occurrence of thin pseudotachylyte veins in the faults described in detail by Martel et al. (1988). Our finding has been corroborated by the identification of other pseudotachylytes within several kilometers of the Bear Creek faults and nearby in the Bear Creek drainage (Kirkpatrick and Shipton, 2008). Here we describe the pseudotachylytes, the associated fault rocks, and the implications for fault deformation mechanisms and seismic slip.

2. Faults of the Bear Creek drainage: previous work

The left-lateral strike-slip faults in Bear Creek cut the 80–90 Ma Lake Edison granodiorite (25% quartz, 40% plagioclase, 25% K-feldspar, and 10% hornblende and biotite; Lockwood, 1975). K-Ar ages of muscovite date the Bear Creek faults at 79 Ma, and these faults have been interpreted as having grown soon after pluton emplacement (Segall et al., 1990). Segall and Pollard (1983b) concluded that the Bear Creek faults developed by slip along pre-existing joints rather than by propagating as shear fractures through unbroken granite. The pre-faulting joints of Bear Creek are filled with hydrothermal mineral assemblages consisting primarily of varying amounts of undeformed quartz, epidote, and chlorite, and have been related to cooling of the plutons (Segall and Pollard, 1983a; Bergbauer and Martel, 1999). Three stages of faulting are recognized. The first stage is marked by "small faults" (Segall and Pollard, 1983b; Martel et al., 1988), which are several millimeters thick and accommodate as much as 2 m of slip. The second stage is marked by "simple fault zones" (Martel et al., 1988), tabular

* Corresponding author. Tel.: +1 650 380 4644; fax: +1 650 725 0979.
E-mail address: wagrif@stanford.edu (W.A. Griffith).

0191-8141/$ – see front matter © 2008 Elsevier Ltd. All rights reserved.
doi:10.1016/j.jsg.2008.05.003

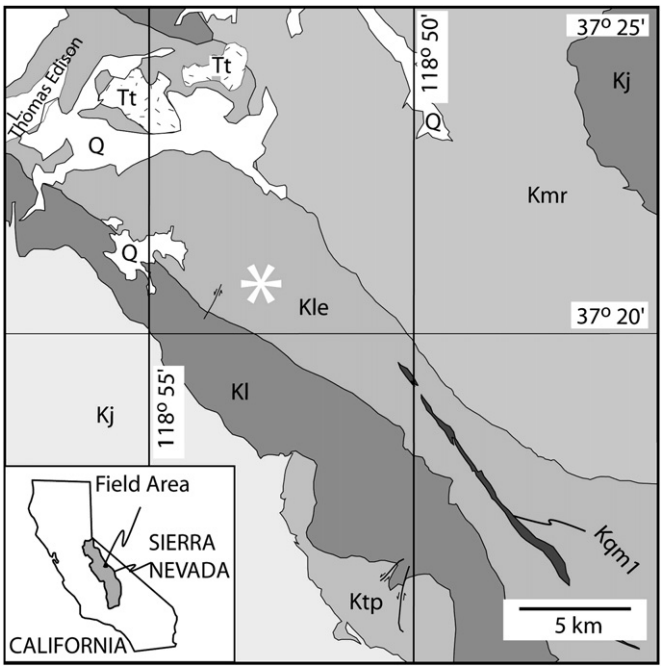

Fig. 1. Simplified geological map of a portion of the Mt. Abbot quadrangle (modified from Bergbauer and Martel, 1999 and Lockwood and Lydon, 1975). The Waterfall site discussed in this paper is indicated by the white star. The main geologic units shown are, from oldest to youngest, unspecified Cretaceous and Jurassic plutons (Kj), the Lamarck granodiorite (Kl), the Mount Givens granodiorite (Kmo), the Lake Edison granodiorite (Kle), Quartz monzonite of Mono Recesses (Kmr), Cretaceous quartz monzonite and granite (Kqm1), Granitic rock of uncertain affinity (Ktp), Tertiary olivine trachybasalt (Tt), and Quaternary deposits (Q).

volumes of moderately to highly fractured rock typically 0.5–3 m thick bounded by former "small faults" millimeters to several centimeters thick. The simple fault zones accommodate as much as 20 m of slip. The third stage is marked by "compound fault zones" (Martel, 1990). These have widths as great as several meters, and accommodate up to 140 m of slip (Pachell and Evans, 2002). Small faults and boundary faults of fault zones of the Bear Creek area are associated with mylonites (Segall and Pollard, 1983b; Segall and Simpson, 1986; Bürgmann and Pollard, 1994), and in some faults the mylonitic fabric has a cataclastic overprint.

Evans et al. (2000) noted that microstructures and geochemical alteration of the Bear Creek faults are similar to mature crustal-scale faults such as the San Andreas as exposed in the San Gabriel Mountains. More recently, Shipton et al. (2006b) compared fault thicknesses measured in the Bear Creek region to the principal slip zone thickness theoretically estimated using typical breakdown energies during earthquake rupture. They concluded that both observations and theoretical estimates support the interpretation that deformation during seismic slip tends to localize in very thin ($\ll$1 cm) zones.

3. Pseudotachylyte-bearing faults

The pseudotachylyte veins were found in left-lateral "small faults" from the "Waterfall Site" of Martel et al. (1988) with ~20 cm strike separation (Fig. 2) that closely approximates the net slip. These millimeter-thick faults contain sub-parallel mylonites, cataclasites, pseudotachylytes and veins of quartz, epidote and zeolite (Fig. 2), that testify to several episodes of fluid infiltration and slip exploiting the same tabular structure. The fault rocks and their overprinting relationships are described and the ambient conditions during faulting based on mineral assemblages and microstructural constraints are estimated.

3.1. Mylonites

Granodiorite–mylonites and quartz mylonites (Fig. 3A) show evidence of recrystallization of biotite, plagioclase, and quartz. Stress-induced quartz-plagioclase myrmekites are developed along grain boundaries between K-feldspar and plagioclase in the wall rock adjacent to mylonites (Fig. 3B) oriented as contractional surfaces relative to the sense of shear of the associated mylonite. The recrystallized plagioclase in the granodiorite–mylonites and myrmekites is oligoclase (Table 1).

Quartz mylonites make up the majority of the thickness of the small faults at most points along strike (e.g. Fig. 2B) and consist of dynamically recrystallized fine-grained (10–100 μm, Fig. 3A) aggregates with an oblique shape fabric, indicative of the same left-lateral sense of shear as in the cataclasites, and a strong crystallographic preferred orientation (Fig. 4). The microstructures show high aspect ratio grain shapes and optically visible subgrains in core-mantle textures (Fig. 3A), characteristic of subgrain rotation recrystallization (Stipp et al., 2002). Electron backscattered diffraction (EBSD) pole figures (Fig. 4) show an oblique single *c*-axis girdle with asymmetry consistent with left-lateral slip.

Mylonites are commonly overprinted along boundaries with the host rock by thin sub-parallel cataclastic layers (Fig. 2A). Mylonitic faults with no cataclastic overprint are similar in appearance to the pseudotachylyte-bearing small faults studied here: they form very sharp discrete boundaries with apparently undeformed host rocks and commonly accommodate over a meter of strike separation in some cases (e.g. Segall and Simpson, 1986).

3.2. Cataclasites and epidote veins

Cataclasites generally form green layers a few millimeters thick in sharp contact with the host rock and the mylonites and typically are associated with epidote-rich veins (e.g. Martel et al., 1988). Cataclasites consist of angular clasts of the host granodiorite and quartz mylonites (Fig. 5A and B), set in a matrix of quartz, K-feldspar, epidote, and minor titanite and chlorite (Fig. 5B).

3.3. Pseudotachylytes

Pseudotachylytes occur as ultra-thin (<300 μm thick) fault veins either forming paired or single slip surfaces oriented sub-parallel to the fault. Pseudotachylytes were found along narrow bands between quartz mylonites and the host rock (Fig. 2), whereas cataclasites were either not present or extremely thin (<100 μm) in samples containing pseudotachylyte (e.g. Fig. 6A and B). Pseudotachylytes were identified based on the presence of typical features summarized by Magloughlin and Spray (1992):

(1) sharp contacts with the host rock and presence of small injection veins (Sibson, 1975) (Figs. 3C and 6A) that typically intrude towards the interior of the fault zone rarely connecting two bounding fault veins (Fig. 2C) (Swanson, 1988);
(2) some embayed clasts of high melting temperature minerals (quartz, feldspar) (Fig. 6C) suggesting assimilation by the melt (e.g. Shand, 1916);
(3) sub-angular clasts of K-feldspar, plagioclase, and quartz in the pseudotachylyte matrix, and absence of hydrous minerals common in the host rocks such as biotite and chlorite (Fig. 6C) and enrichment of Fe, Mg, K, and Loss On Ignition (interpreted as water), along with depletion of Si and Ca, of the pseudotachylyte matrix compared to the host rocks (granodiorite and mylonites, Table 1). This results from selective melting of

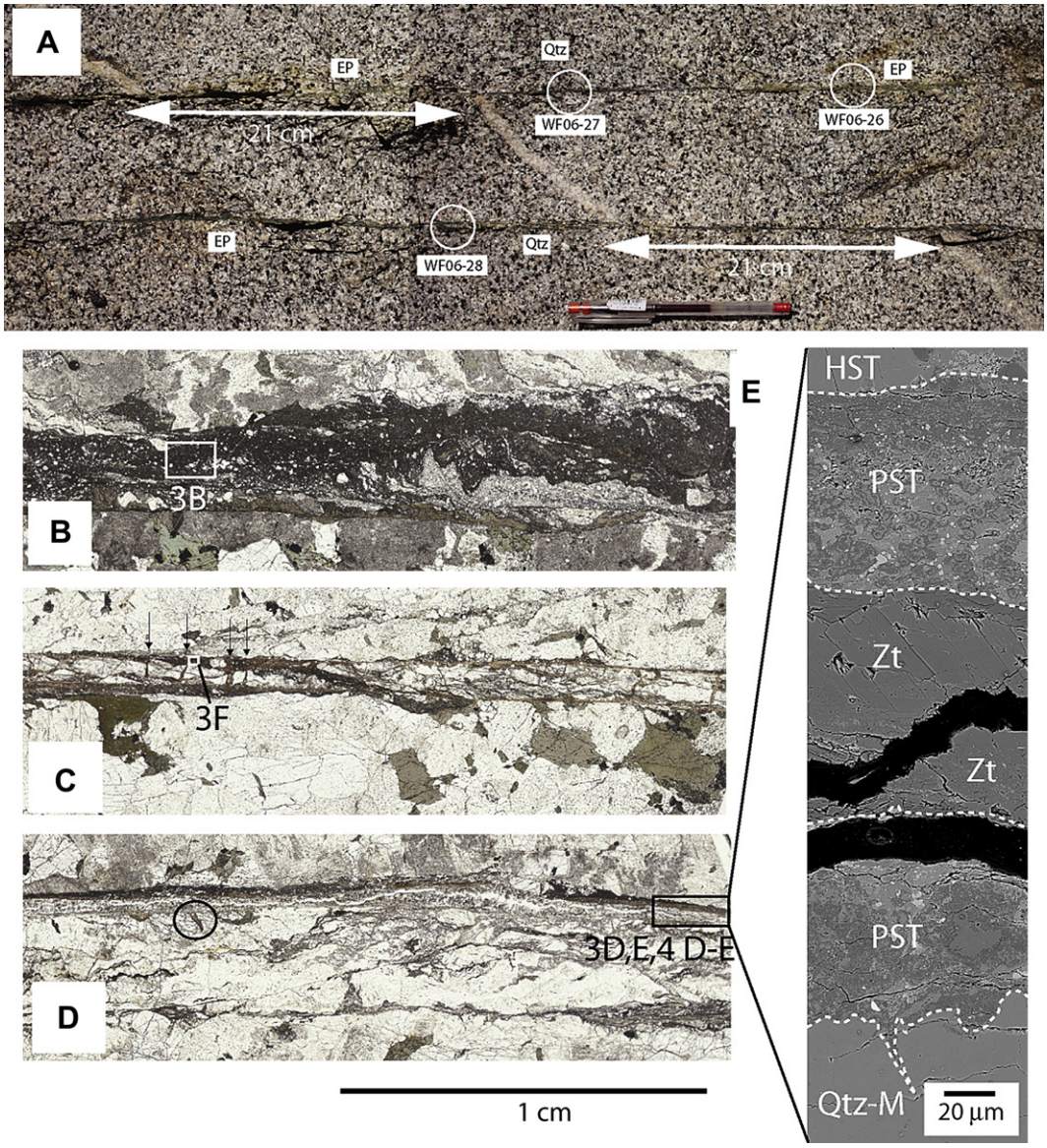

Fig. 2. (A) Faults from which pseudotachylyte samples were taken. On the subhorizontal outcrop, strike separation, measured from offset of subvertical aplite dike is ~21 cm. Slickenlines and mineral stretching lineations on mylonites plunge less than 20° across the outcrop. White circles indicate locations of samples shown in B, C, and D of this figure, respectively. Ep and Qtz refer to alternating zones of dominant mineral fillings (epidote cataclasite and quartz mylonite) along each fault. Looking down, top to S; pen (13 cm long) for scale. (B) and (C) Optical microscope images under plane polarized light of "small fault" samples. (B) Sample WF06-26. The dominant filling is epidote-rich cataclasite (dark material). Lighter colored mineral filling is reworked quartz mylonite. The white box indicates the location of Fig. 3B. (C) Sample WF06-27. Dark slip surfaces bound pre-existing quartz mylonites. Black arrows point out small pseudotachylyte injection veins connecting slip surfaces. (D) Sample WF06-28. The majority of mineral fill is quartz mylonite, which is overprinted on the edges of the fault by dark bands consisting of cataclasite, pseudotachylyte, and zeolite. Black circle indicates an injection vein. (E) Overview of pseudotachylyte vein in relationship to zeolite, quartz mylonites, and host rock (BSE-SEM). Black areas are holes in the thin section.

iron-rich, low melting temperature minerals, biotite and hornblende (e.g. Sibson, 1975; Maddock, 1992; Spray, 1992);

(4) spherulites (Fig. 6D and E) characterized by a central clast surrounded by alternating K-feldspar and plagioclase-rich rims, typical of pseudotachylytes from granitoid rocks (e.g. Lin, 1994; Di Toro and Pennacchioni, 2004);

(5) flow structures (Fig. 6C);

(6) spherical Fe-rich grains, interpreted as solidified droplets of oxide-rich melt (Fig. 6C). Since oxide-rich melts are immiscible in silicate-rich melts (Philpotts, 1990), the presence of spherical Fe-rich grains suggests non-equilibrium frictional melting (as observed in experimental pseudotachylytes, Di Toro et al., 2006, unpublished data).

These features are typical of pseudotachylytes described in granitoid rocks (e.g. Di Toro and Pennacchioni, 2004). The pseudotachylyte matrix is very fine-grained: individual grains are not visible within the resolution limits (200 nm) of the SEM. The composition of the pseudotachylyte matrix is intermediate between di- and tri-octahedral mica, and contains roughly 5–6% water (Table 1). Titanite, and less commonly epidote, occur as overgrowths in the pseudotachylyte matrix (Fig. 3D and E).

3.4. Zeolite veins

Thin (~200 mm) zeolite-filled veins are common within the small faults. The veins are sub-parallel to the faults, and locally cut across the mylonites, cataclasites and pseudotachylytes. (Fig. 6A, B, D–F). Zeolite filling is always undeformed with prismatic crystals of stilbite–heulandite (Table 1) roughly oriented with the long axis orthogonal to the vein. The combination of cross-cutting

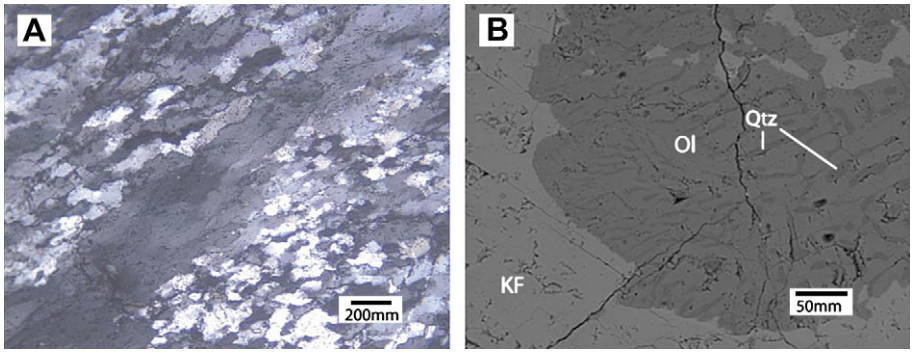

Fig. 3. (A) Dynamically recrystallized aggregate of quartz in a sheared vein within a small fault showing a clear shape preferred orientation of grains. The sense of shear is left-lateral. Crossed polars. (B) SEM backscattered image of a myrmekite developed in granodiorite–mylonite between a potassium feldspar (KF, SW corner) and a plagioclase grain (NE corner Qtz = quartz; Ol = oligoclase (sample WF06-28, BSE-SEM)).

relationships and lack of deformation of zeolite minerals suggest that the zeolite veins post-date fault slip.

4. Discussion

4.1. Ambient conditions during ductile-to-brittle deformation

A conceptual model for the microstructural evolution of shearing described in this study is presented in Fig. 7 and placed within the context of the macrostructural model of fault development described by Martel et al. (1988). The field and microstructural observations in the Lake Edison granodiorite indicate a succession of crystal-plastic to brittle deformation events localized along the single set of cooling joints during decreasing temperature and systematic left-lateral shearing. At an early high temperature stage, joints opened and were filled with discontinuous quartz veins. Subsequent shearing localized within the quartz veins and produced quartz mylonites. Granodiorite–mylonites developed adjacent to quartz mylonites as shearing spread laterally into the host rock. The temperature during crystal-plastic deformation is estimated at $T > 400\,^{\circ}C$ based on: (1) the synkinematic recrystallization of biotite and oligoclase in the mylonites, and the development of stress-induced oligoclase-bearing myrmekites; and (2) the crystallographic preferred orientation of the recrystallized quartz within mylonites, consistent with a regime of subgrain rotation recrystallization and typical of greenschist facies metamorphic assemblages (e.g. Stipp et al., 2002).

The cataclasites formed at relatively deep conditions in the brittle field as suggested by the propylitic alteration mineral assemblages associated with cataclasites and epidote veins (e.g. Guilbert and Park, 1986). This mineral assemblage suggests temperatures in the range 200–300 °C. Assuming a geothermal gradient of 25–30 °C/km, this corresponds to a depth range between 7 and 10 km. This is consistent with published estimates of pluton emplacement by Al-in-hornblende geobarometry of 1–4 kbars corresponding to depths of 4–15 km (Ague and Brimhall, 1988). Therefore the cataclasites formed after cooling of pluton to the host rock temperature and before exhumation of the intrusive rocks. The static growth of epidote on the pseudotachylyte matrix (Fig. 6E) indicates that these ambient conditions persisted during pseudotachylyte-producing seismic slip along the faults. The overprint of the fault assemblage by non-sheared zeolite veins suggests that fault slip was concluded at temperatures above 200 °C (Deer et al., 1992).

4.2. Estimates of seismic slip on Bear Creek faults

Within a total fault thickness of less than 0.5 cm and an offset of approximately 20 cm (Fig. 2), the small faults preserve a multi-stage record of deformation interpreted as aseismic creep (mylonites), brittle shearing (cataclasites), seismic slip (pseudotachylytes), and further cooling and opening (zeolites). Both the mesoscale and microstructural indicators suggest the same left-lateral sense of shear along the small faults during the crystal-plastic (i.e. mylonites) and brittle (i.e. cataclasites) deformations. The dominant fault mineral fillings alternate along strike between cataclasite (epidote) and mylonite (quartz, biotite) (Fig. 2). The pseudotachylytes discussed here were found at the interface between quartz mylonites and the host rock and were associated with very thin ($\sim$100 μm) cataclasites, whereas sections of the fault made up principally of thicker $\sim$1 cm cataclasite did not contain evidence of pseudotachylyte. This suggests that the spatial

Table 1
Oxide weight percents determined by microprobe analysis of major constituents of pseudotachylyte, cataclasite, and host rock

(%)	Myrmekite plagioclase (9)		plagioclase (7)		Epidote (9)		Zeolite (8)		Host rock biotite (3)		Pseudotachylyte matrix (9)		Bulk host rock[a]
	wt %	s.d.	wt %	s.d.	wt %	s.d.	wt %	s.d.	wt %	s.d.	wt %	s.d.	wt %
SiO_2	62.96	0.27	61.93	0.55	36.71	0.53	59.63	1.09	38.12	0.38	41.56	1.74	66.7
TiO_2	0	0	0.04	0.03	0.2	0.21	0	0	1.45	0.11	0.56	0.7	0.44
Al_2O_3	23.33	0.15	24.3	0.32	22.39	0.35	16.04	0.44	15.99	0.23	21.04	1.62	16.1
FeO	0.01	0.3	0.14	0.05	13.46	0.86	0.02	0.03	16.6	0.02	11.92	1.3	3.8
MnO	0.02	0.03	0.02	0.02	0.46	0.16	0.01	0.02	0.45	0.05	0.26	0.08	0.08
MgO	0.03	0.01	0.02	0.01	0.2	0.19	0	0.01	14.06	0.12	9.09	1.81	1.5
CaO	4.86	0.25	5.43	0.38	22.05	0.78	8.3	0.19	0.02	0.03	0.81	1.09	3.5
Na_2O	8.78	0.1	8.49	0.14	0.03	0.02	0.64	0.17	0.09	0.05	0.1	0.02	3.5
K_2O	0.15	0.08	0.29	0.16	0.16	0.08	0.01	0.02	9.65	0.26	9.44	0.43	3.7
Oxide totals	100.11	0.49	100.66	0.52	95.73	1.77	84.81	1.07	96.42	0.86	94.79	1.4	100

[a] Bulk host rock compositions from Lockwood (1975). Rock composition is roughly constant (+/−1%) across the Lake Edison granodiorite.

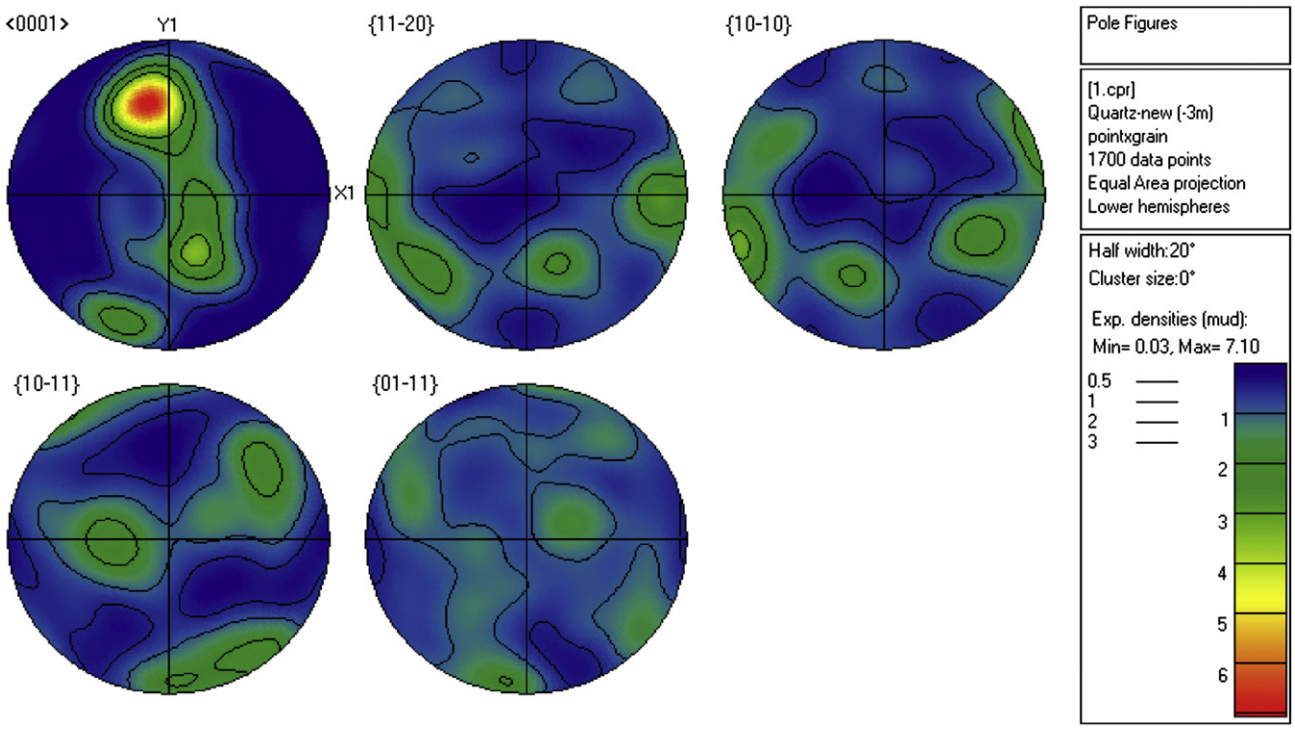

Fig. 4. Electron backscattered diffraction (EBSD) analysis of the crystallographic orientations of the quartz mylonite sample WF06-04. Pole figure with color coded and contoured pole-densities expressed as *x*-times the mean unit density of a uniform distribution. It is particularly evident that the poles to the {11–20} planes (i.e. *a*-axes) are preferentially aligned with the shear plane, whereas the poles to the {10–10} prism planes and the planes of the {10–11} rhombohedron are preferentially aligned with the oblique foliation. Overall, the *c*-axis distribution pattern describes a girdle with a week asymmetry. X_1 is the shear plane, and the shear sense is right-lateral. The single girdle of the *c*-axis typical of greenschist facies quartz mylonites (Stipp et al., 2002).

occurrence of pseudotachylyte may be related to the dominant mineralogy of the fault filling. Pseudotachylyte veins are less than 300 μm in thickness in all samples, and the entire package of pseudotachylyte and thin cataclasites that occurs at the interface between quartz mylonites and granodiorite host rock generally does not exceed about 0.5 mm. Such extreme slip localization has been shown theoretically to be promoted by thermal weakening mechanisms (e.g. Rice, 2006).

Most small faults are segmented over strike distances of a few meters to a few tens of meters reflecting the original segmentation of precursor joints (e.g. Martel et al., 1988). Crosscut markers up to a few meters away from tips indicate that small faults accommodate offsets corresponding to a very high ratio between displacement and length (Christiansen and Pollard, 1997). These high displacement/length ratios are not compatible with purely elastic deformation of the host rock during cataclasis within the faults and can only be only accomplished by slip under predominantly crystal-plastic deformation conditions (Pennacchioni, 2005). In this case the high displacement gradients along faults (and especially near fault tips) are principally accommodated by the development of a high temperature fabric in the granodiorite host rock, especially in contractional domains near steps and tips and to a lesser extent by opening of quartz veins in extensional domains. The lower temperature epidote-bearing extensional veins developed at small fault tips are coeval with the cataclasites (e.g. Segall and Pollard, 1983b). These veins are only capable of transferring a small cumulative slip on the order of a few centimeters (e.g. Fig. 6 of Bürgmann and Pollard, 1994): a small fraction of the total offset along these faults as determined from offset markers. Because of the complex microstructural history of the faults and the evidence that shear took place plastically prior to the brittle conditions recorded by cataclasites and pseudotachylytes, the contribution of

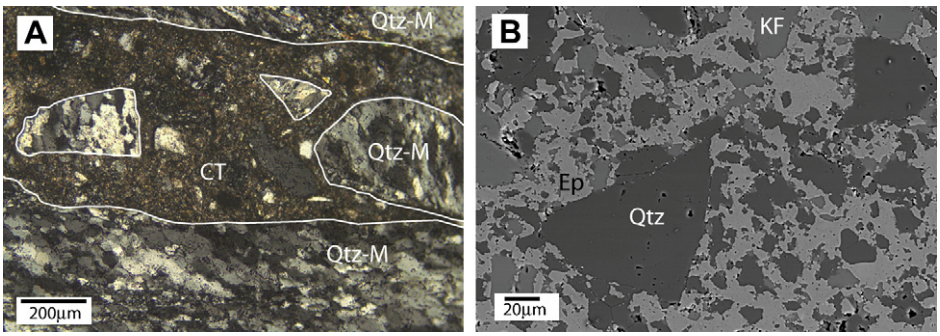

Fig. 5. Optical and SEM images of cataclasite textures and cross-cutting relationships. (A) Cataclasite (CT) containing quartz mylonite clasts cuts quartz mylonite (Qtz-M) in a boundary fault (WF06-24, optical microscope, crossed polars) (B) Cataclasite with clasts of angular to sub-angular quartz and potassium feldspar (KF) cemented by epidote (Ep) (sample WF06-26, BSE-SEM).

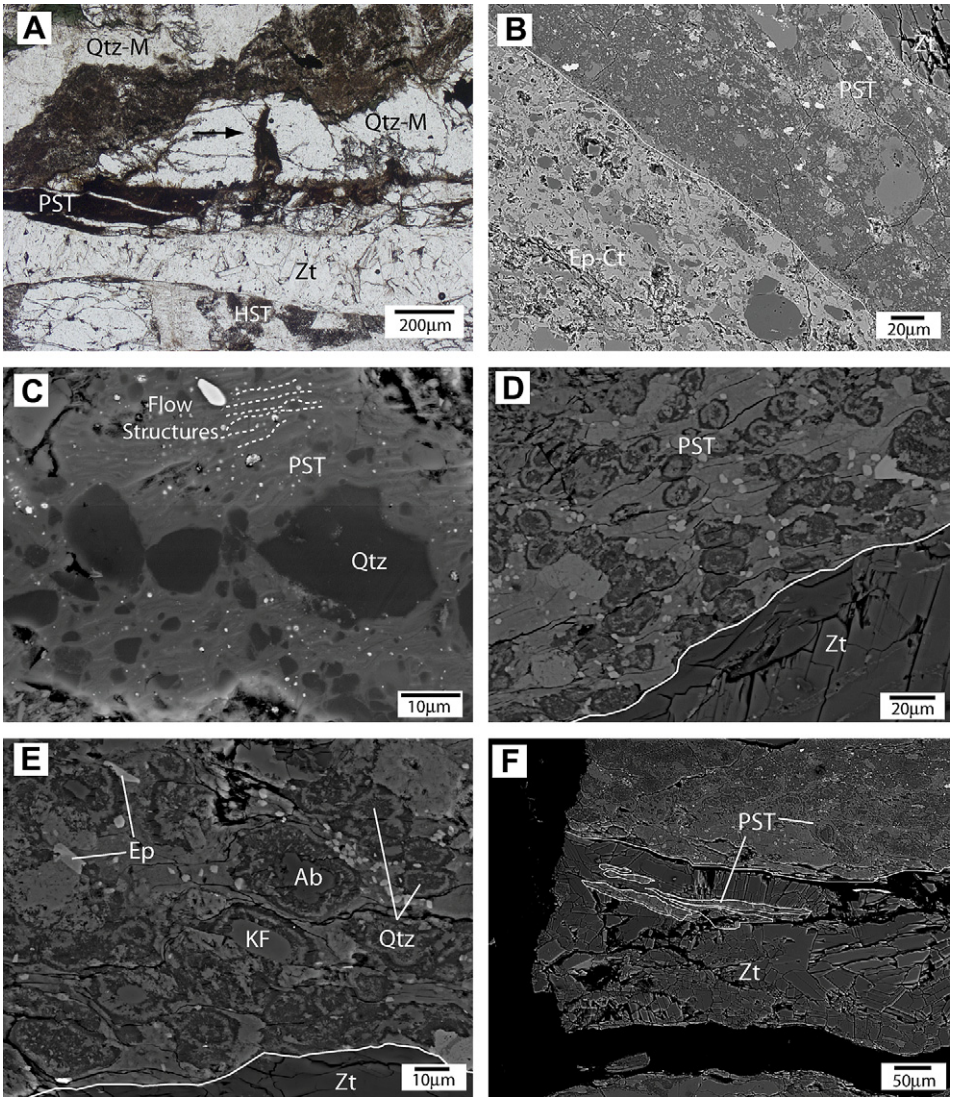

Fig. 6. Optical and SEM images of pseudotachylyte textures and cross-cutting relationships. (A) Pseudotachylyte (PST) fault vein cutting a quartz mylonite (Qtz-M). Arrow points to a pseudotachylyte injection vein. A sub-parallel zeolite vein (Zt) cuts both the PST and Qtz-M (sample WF06-27, optical microscope, plane polarized light). (B) Contact between pseudotachylyte and epidote-rich cataclasite in sample WF06-28. Pseudotachylyte development may have post-dated or been coeval with cataclasis. (BSE-SEM). (C) PST with rounded, slightly embayed clasts. PST matrix shows faint flow structures. Rounded bright-white blobs (indicated by white arrow) are Fe-rich bubbles (sample WF06-27, BSE-SEM). (D) PST with spherulitic texture cut by a Zt vein. Small bright crystals are titanite (sample WF06-28, BSE-SEM). (E) PST with spherulites cored by plagioclase (Pl), potassium feldspar (KF), and quartz (Qtz). Note post-solidification epidote overgrowths (sample WF06-28, BSE-SEM). (F) Slivers of pseudotachylyte vein contained in zeolite vein in sample WF06-28. Note that pseudotachylyte post-dated mylonitic deformation and predated zeolite formation (BSE-SEM).

seismic slip to total offset across the fault is interpreted to be very small. These small values suggest that extrapolating values of seismic slip from measured values of total offset in the field may produce significant overestimations (e.g. Shipton et al., 2006a).

Because some of the Bear Creek small faults are exposed along their entire lengths (i.e. from tip to tip), measuring the slip corresponding to seismic events on these faults could be used to constrain earthquake source parameters such as static stress drop and seismic moment (e.g. Kanamori and Heaton, 2000; Scholz, 2002). This has not been possible for other well-studied pseudotachylyte-bearing faults because of the complex network of fractures and faults, incomplete exposures that impede the determination of the fault length, or lack of offset markers (e.g. Sibson, 1975; Swanson, 1992; Di Toro et al., 2005; Sibson and Toy, 2006). Zechmeister et al. (2007) used an empirical scaling relationship, $d = 436a^2$, that relates pseudotachylyte fault vein thickness, a, to slip, d, from (Sibson, 1975) to estimate the slip responsible for pseudotachylytes along faults of the Dora Maira Massif in the Italian Alps. In this relationship, the empirical constant 436 must have dimensions of L^{-1} to make the equation dimensionally homogeneous. This relationship may provide a fit to data for the faults studied by Sibson (1975), but is not meaningful from a physical point of view because it does not contain the physical quantities relevant to frictional heating and melting. As such it is not appropriate to extrapolate this relationship to faults formed in other locales where the physical quantities may take on different values. We estimate lower and upper bounds on the slip based on physically meaningful relationships including: (1) conductive heat transfer; and (2) the local seismic energy budget.

4.2.1. Conductive heat transfer

Since the ~200 μm thick pseudotachylyte fault veins are spatially associated with thin cataclasite layers, it is reasonable to assume that the pseudotachylytes were produced by shear across such thin zones. In order to place a lower bound on the slip, we follow Cardwell et al. (1978) and approximate the temperature rise

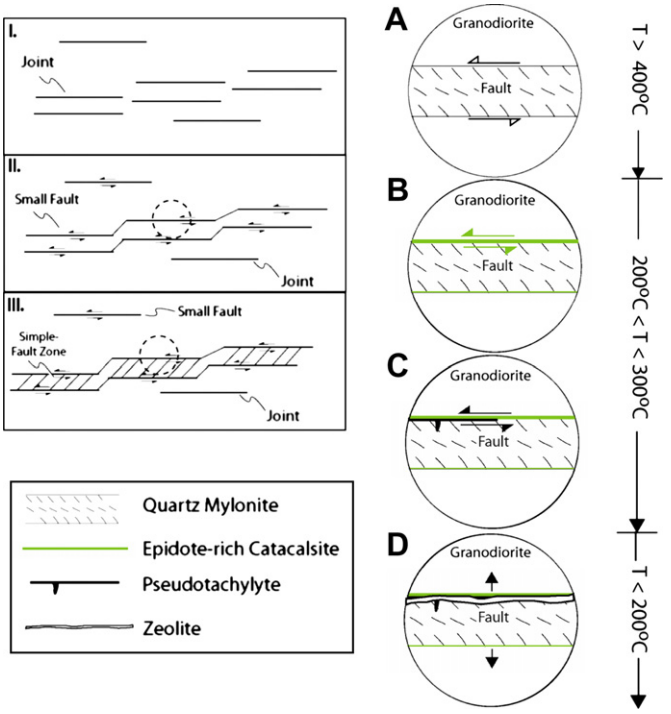

Fig. 7. Conceptual model of macroscopic and microscopic evolution of faults in Bear Creek. I–III correspond to the macroscopic evolution of faults suggested by Martel et al. (1988), where in stage I joints form in response to thermal stresses; stage II is marked by slip nucleation along joints and subsequent linkage to form small faults; and in stage III simple fault zones composed of paired small faults linked by secondary fractures form due to interaction of neighbouring faults. Martel (1990) also proposed a fourth stage of development in which simple fault zones coalesce to form large, complex fault zones, but the fourth stage has been omitted from this figure for simplicity. Dashed circles in II and III indicate the location of A, B, C, and D. A–D represent the microstructural evolution of faults from the time that shearing commences to the transition from shearing deformation to zeolite veining. (A) Quartz precipitated in dilatational regions along faults is sheared at temperatures greater than 400 °C producing quartz mylonites. (B) Boundaries between mylonites and granodiorites are filled with epidote veins and reactivated by cataclasites cemented by epidote. Locally cataclasites and epidote veins cut across mylonites. (C) Thin, discontinuous pseudotachylyte veins form due to seismic slip, and locally cut mylonites and cataclasites. (D) The termination of shear deformation is signified by opening of faults and zeolite mineralization.

due to shear across a fault of finite thickness. Assuming that slip takes place as constant velocity shear distributed across a dry principal slip zone of finite thickness w, the governing equation for one dimensional conductive heat transport is:

$$\rho c_p \frac{\partial T}{\partial t} = k \frac{\partial^2 T}{\partial x^2} + A(x,t) \tag{1}$$

where k is the thermal conductivity of granodiorite (2.79 $Wm^{-1}K$, Clark, 1966), ρ is the granodiorite mass density (2700 kg m^{-3}), c_p is the specific heat for granodiorite (1200 J kg^{-1} K^{-1} for granodiorite, Di Toro and Pennacchioni, 2004), and t is the time sliding occurs at a point along the fault, and $A(x,t)$ is the frictional heat source distributed evenly across the zone of shearing, w, given by:

$$A(x,t) = \frac{\tau d}{wt}\left[H\left(x+\frac{w}{2}\right) - H\left(x+\frac{w}{2}\right)\right] \tag{2}$$

where $H()$ is the Heaviside step function, d is the total slip, and τ is the shear stress on the fault calculated from the equation $\tau = \mu\sigma_n$ Here σ_n is the effective normal stress on the fault and μ is the sliding friction coefficient. We use the value $\mu = 0.4$, equal to that used by Lachenbruch (1980). This value is lower than "Byerlee" friction ($\mu \approx 0.6$–0.85) (Byerlee, 1978) and higher than values ($\mu < 0.1$) from

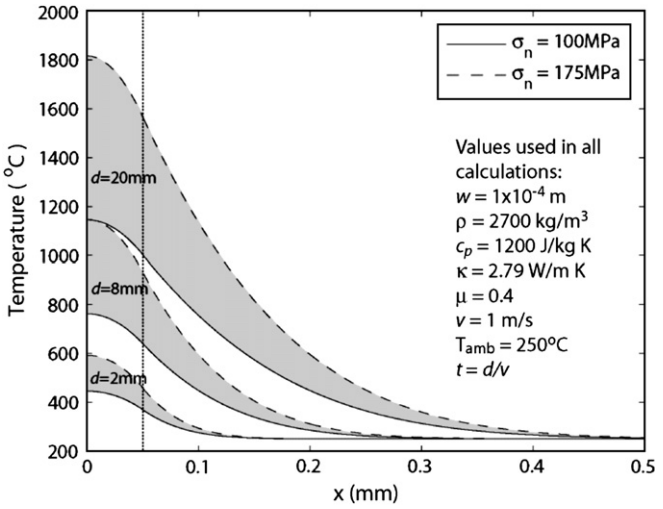

Fig. 8. Temperature profiles at time $t = d/v$ as a result of constant velocity shear across a fault zone of 100 μm thickness. The half width ($w/2$) of the fault zone is indicated by the vertical dotted line at $x = 50$ μm. Ranges (gray) of temperature profiles are shown for coseismic slips of $d = 2$, 8, and 20 mm. The upper curve for each range (dashed line) is for the case of $\sigma_n = 175$ MPa and the lower curve (solid line) represents $\sigma_n = 100$ MPa. All temperature profiles decay to the ambient temperature ($T_{amb} = 250$ °C) within 0.5 mm of the center of the shearing zone. Melting temperatures, considering heat loss only by conduction in a pore-fluid-free fault zone, can be reached for slip $d < 1$ cm.

dynamic friction experiments of Di Toro et al. (2006) where low values were largely a product of melt lubrication. We consider values for σ_n ranging from 100 MPa to 175 MPa corresponding to a range of possible effective stress values at a depth of ~7 km. Cardwell et al. (1978) showed that the temperature at any point perpendicular to the fault at time t is given by:

$$T(x,t) = T_{amb} + \frac{\tau d}{2\rho c_p wt}\int_0^t \left[\operatorname{erf}\left(\frac{x+(w/2)}{\sqrt{4\kappa(t-t_0)}}\right) - \operatorname{erf}\left(\frac{x-(w/2)}{\sqrt{4\kappa(t-t_0)}}\right)\right] dt_0 \tag{3}$$

in this equation, $T(x,t)$ is the temperature profile, T_{amb} is the ambient host rock temperature (250 °C, see Section 4.1), κ is the thermal diffusivity ($k/\rho c_p$), and t_o is an integration variable. Temperature profiles for earthquakes of varying slip for prescribed material parameters for the host granodiorite are shown in Fig. 8. It should be noted that the commonly cited maximum temperature rise at the center of the shearing zone given by

$$T_{max} = T_{amb} + \frac{\tau d}{\rho c_p (\pi\kappa t)^{1/2}} \tag{4}$$

is not valid for this case, as it assumes that negligible heat will be lost from the shearing zone during the slip event (i.e. the conduction length during the event, $(\kappa t)^{1/2} \ll w$). For the case of $d = 20$ mm (Fig. 7) $(\kappa t)^{1/2} = 130$ μm, on the same order as the width of the shearing zone w. Assuming a melting temperature of 1000–1200 °C (e.g. Di Toro and Pennacchioni, 2004), Eq. (3) predicts a minimum slip of $d \leq 1$ cm to initiate melting.

4.2.2. Local seismic energy budget

The upper bound for the slip during an individual earthquake can be estimated by calculating the energy necessary to produce a volume of melt with average thickness equal to 200 μm, that of pseudotachylyte veins typical of these faults (e.g. Sibson, 1975; Di Toro et al., 2005). An expression for the average slip d necessary to

produce a melt vein of thickness a can be found by rearranging Eq. (9) of Di Toro et al. (2005):

$$d = \frac{\rho a}{\tau}[(1-\phi)H + c_p(T_{melt} - T_{amb})] \quad (5)$$

in this equation, ϕ is the percentage of unmelted clasts in the pseudotachylyte, H is the latent heat of fusion, and a is the average thickness of the pseudotachylyte fault vein. In the interest of finding the upper bound for slip, we can simplify this equation by assuming that all of the pseudotachylyte vein is melt (i.e. $\phi = 0$), so Eq. (5) becomes:

$$d = \frac{\rho a}{\tau}[H + c_p(T_{melt} - T_{amb})] \quad (6)$$

using a value for the latent heat of fusion ($H = 3.28 \times 10^5$ J/kg) from Di Toro et al. (2005) and the values above for τ, c_p, and ρ, Eq. (6) yields an upper bound on fault slip during a pseudotachylyte generating rupture of $d = 7$ cm.

These physically based analyses predict that the slip corresponding to a single, melt-producing earthquake on the small faults of Bear Creek would have been approximately 1–7 cm. This range in slip is less than the total offset of 21 cm and is consistent with the observation that most of this cumulative slip is accommodated by mylonites prior to seismic slip.

The evidence presented in this paper indicates that the coseismic slip may only constitute a small fraction of the total offset as measured on small faults in the Bear Creek area; the majority of slip is accumulated in the crystal-plastic regime. Consequently, any attempt to establish empirical scaling laws relating fault slip to thickness (e.g. Scholz, 1987), or slip to fault length (e.g. Scholz et al., 1993; Cladouhos and Marrett, 1996) will, on these types of faults lead to misleading results unless the total slip is appropriately partitioned among all the deformation mechanisms that accommodate slip from plastic to brittle to seismic. This observation is consistent with the argument of Evans (1990) that deviations from power-law scaling relationships may be due to rock type, structural setting, and processes responsible for the fault development. This study is a demonstration of Evans' third point: the deformation path of faults throughout their development is non-unique. Because slip can be accommodated by any number of deformation mechanisms during fault evolution, the presence of pseudotachylyte does not imply that deformation can be attributed to seismic slip, or even brittle slip, alone.

4.3. Insights from other locales

The succession of structures within the faults, the host rock mineralogy, and the estimated ambient conditions of faulting in the Bear Creek area are similar to those described from the Adamello pluton of the Italian Alps by Pennacchioni et al. (2006). Faults in both locales formed at seismogenic depths during cooling of the host granitoid rocks, and slip events nucleated along pre-existing networks of sub-parallel joints. In both cases joints are first exploited as very discrete mylonites, accommodating most of the total offset, and then as cataclasites associated with a final event of frictional melting. This deformation sequence may be characteristic of cooling granitic plutons emplaced in seismogenically active regions.

There remain noteworthy differences between the faults of these locales. Despite similar conditions of nucleation and initial growth, a bifurcation in the evolutionary paths of these fault systems is evidenced by one obvious difference: faults of the Adamello batholith contain abundant macroscopic pseudotachylyte-filled veins, whereas pseudotachylytes in faults of the Bear Creek area are largely of the thin microscopic variety discussed above.

5. Conclusions

The Bear Creek faults preserve a record of deformation ranging from aseismic ductile shearing through cataclasis and finally pseudotachylyte generation, all within an extremely thin (<1 cm) shear zone. Seismic ruptures exploited pre-existing discontinuities formed as opening fractures during pluton cooling that later were sheared producing mylonitic textures; in the final stage seismic slip and associated frictional melting occurred at temperatures near ~250 °C.

Occurrences of pseudotachylytes within very thin (sub-millimeter thickness) shear zones in faults and the notable lack of pseudotachylytes within thicker cataclasites supports the interpretation of extreme slip localization during seismic slip. Additionally, because the volume of melt in these faults is very small, and multiple lines of evidence suggest that only a small fraction of the total measured offset along these faults accumulated coseismically, the extrapolation of data collected from exhumed seismic faults in granitic rocks to earthquake mechanics models must be done with some caution. Seismic slip values are likely much smaller than slip measured in the field using offset markers.

The pseudotachylytes found along the Bear Creek faults are very difficult to identify even in thin section, and are impossible to identify in the field in most cases, whereas the vast majority of pseudotachylytes described in the literature are visible in outcrop. The elusive nature of these pseudotachylytes suggests that frictional melting may be more common than previously thought in similar faults.

Acknowledgements

The authors would like to thank S.J. Martel for an insightful introduction to the Bear Creek outcrops, J.C. White and D. Cowan for constructive reviews of this manuscript, R. Spiess for the EBSD analysis (L. Peruzzo and L. Tauro for sample preparation and SEM facilities) in Padova, and B. Jones at Stanford for his microprobe expertise. This work was supported financially by the Rock Fracture Project at Stanford and by the Cariparo grant and PRIN 2005044945 at Padova.

References

Ague, J.J., Brimhall, G.H., 1988. Magmatic arc aysymmetry and distribution of anomalous plutonic belts in the batholiths of California: effects of assimilation, crustal thickness, and depth of crystallization. Geological Society of America Bulletin 100, 912–927.

d'Alessio, M.A., Martel, S., 2004. Fault terminations and barriers to fault growth. Journal of Structural Geology 26, 1885–1896.

Bergbauer, S., Martel, S.J., 1999. Formation of joints in cooling plutons. Journal of Structural Geology 21, 821–835.

Bürgmann, R., Pollard, D.D., 1994. Strain accommodation about stick-slip fault discontinuities in granitic rock under brittle-to-ductile conditions. Journal of Structural Geology 16, 1655–1674.

Byerlee, J., 1978. Friction of rocks. Pageoph 116, 615–626.

Cardwell, R.K., Chinn, D.S., Moore, G.F., Turcotte, D.L., 1978. Frictional heating on a fault zone with finite thickness. Geophysical Journal of the Royal Astronomical Society 52, 525–530.

Christiansen, P.P., Pollard, D.D., 1997. Nucleation, growth and structural development of mylonitic shear zones in granitic rock. Journal of Structural Geology 19, 1159–1172.

Cladouhos, T.T., Marrett, R., 1996. Are fault growth and linkage models consistent with power-law distributions of fault lengths? Journal of Structural Geology 18, 281–293.

Clark, S.P., 1966. Thermal conductivity. In: Clark, S.P. (Ed.), Handbook of Physical Constants. Geological Society of America, Memoir, vol. 97, pp. 459–482.

Cowan, D., 1999. Do faults preserve a record of seismic slip?-a field geologist's opinion. Journal of Structural Geology 21, 2703–2719.

Deer, W.A., Howie, R.A., Zussman, J., 1992. An Introduction to the Rock-Forming Minerals. Longman. Hollow.

Di Toro, G., Hirose, T., Nielsen, S., Pennacchioni, G., Shimamoto, T., 2006. Natural and experimental evidence of melt lubrication of faults during earthquakes. Science 311, 647–649.

Di Toro, G., Pennacchioni, G., 2004. Superheated friction-induced melts in zoned pseudotachylytes within the Adamello tonalites (Italian Southern Alps). Journal of Structural Geology 26, 1783–1801.

Di Toro, G., Pennacchioni, G., Teza, G., 2005. Can pseudotachylytes be used to infer earthquake source parameters? An example of limitations in the study of exhumed faults. Tectonophysics 402, 3–20.

Evans, J.P., 1990. Thickness–displacement relationships for fault zones. Journal of Structural Geology 12, 1061–1065.

Evans, J.P., Shipton, Z.K., Pachell, M.A., Lim, S.J., Robeson, K., 2000. The structure and composition of exhumed faults, and their implications for seismic processes. In: Bokelmann, G., Kovach, R.L. (Eds.), Third Conference on Tectonic Problems of the San Andreas Fault System, vol. 21. Stanford University Publications, pp. 67–81.

Guilbert, J.M., Park, C.F., 1986. The Geology of Ore Deposits. Freeman and Company, New York.

Kanamori, H., Heaton, T., 2000. Microscopic and macroscopic physics of earthquakes. In: Rundle, J., Turcotte, D., Klein, W. (Eds.), Geocomplexity and the Physics of Earthquakes. Geophysical Monograph, vol. 20. American Geophysical Union, Washington, D.C., pp. 127–141.

Kirkpatrick, J.D., Shipton, Z.K., 2008. Spatial and temporal heterogeneity of exhumed seismogenic faults; implications for seismic slip. European Geophysical Union Geophysical Abstracts 10 EGU2008-A-09126.

Lachenbruch, A.H., 1980. Frictional heating, fluid pressure, and the resistance to fault motion. Journal of Geophysical Research 85, 6097–6112.

Lin, A., 1994. Glassy pseudotachylytes from the Funyun Fault Zone, Northwest China. Journal of Structural Geology 16, 71–83.

Lockwood, J., 1975. Mount Abbot Quadrangle, Central Sierra Nevada, California – Analytic Data. Geological Survey Professional Paper 774-C.

Lockwood, J.P., Lydon, P.A., 1975. U.S. Geologic map of the Mount Abbot Quadrangle, California. Geological Survey Geologic Quadrangle GQ-1155 scale 1:62,500.

Maddock, R., 1992. Effects of lithology, cataclasis and melting on the composition of fault-generated pseudotachylytes in Lewisian gneiss, Scotland. Tectonophysics 204, 261–278.

Martel, S.J., 1990. Formation of compound strike-slip fault zones, Mount Abbot quadrangle, California. Journal of Structural Geology 12, 869–882.

Martel, S.J., Pollard, D.D., 1989. Mechanics of slip and fracture along small faults and simple strike-slip fault zones in granitic rock. Journal of Geophysical Research 94, 9417–9428.

Martel, S.J., Pollard, D.D., Segall, P., 1988. Development of simple strike-slip fault zones, Mount Abbot Quadrangle, Sierra Nevada, California. Geological Society of America Bulletin 100, 1451–1465.

Pachell, M.A., Evans, J.P., 2002. Growth, linkage, and termination processes of a 10-km-long, strike-slip fault in jointed granite: the Gemini fault zone, Sierra Nevada, California. Journal of Structural Geology 24, 1903–1924.

Pennacchioni, G., 2005. Control of the geometry of precursor brittle structures on the type of ductile shear zone in the Adamello tonalites, Southern Alps (Italy). Journal of Structural Geology 27, 627–644.

Pennacchioni, G., Di Toro, G., Brack, P., Menegon, L., Villa, I.M., 2006. Brittle-ductile-brittle deformation during cooling of tonalite (Adamello, Southern Italian Alps). Tectonophysics 427, 171–197.

Philpotts, A.R., 1990. Principals of Igneous and Metamorphic Petrology. Prentice Hall, Englewood Cliffs.

Rice, J.R., 2006. Heating and weakening of faults during earthquake slip. Journal of Geophysical Research 111, doi:10.1029/2005JB004006.

Scholz, C.H., 1987. Wear and gouge formation in brittle faulting. Geology 15, 493–495.

Scholz, C.H., 2002. The Mechanics of Earthquakes and Faulting. Cambridge University Press, Cambridge.

Scholz, C.H., Dawers, N.H., Yu, J.Z., Anders, M.H., 1993. Fault growth and fault scaling laws: preliminary results. Journal of Geophysical Research 98, 21951–21961.

Segall, P., McKee, E.H., Martel, S.J., Turrin, B.D., 1990. Late Cretaceous age of fractures in the Sierra Nevada batholith, California. Geology 18, 1248–1251.

Segall, P., Pollard, D.D., 1983a. Nucleation and growth of strike slip faults in granite. Journal of Geophysical Research 88, 555–568.

Segall, P., Pollard, D.D., 1983b. Joint formation in granitic rock of the Sierra Nevada. Geological Society of America Bulletin 94, 563–575.

Segall, P., Simpson, C., 1986. Nucleation of ductile shear zones on dilatant fractures. Geology 14, 56–59.

Shand, S.J., 1916. The pseudotachylyte of the Parijs (Orange Free State) and its relation to "trap-shotten gneiss" and "flinty crush rock". Quarterly Journal of the Geological Society of London 72, 198–221.

Shipton, Z.K., Evans, J.P., Abercrombie, R.E., Brodsky, E.E., 2006a. The missing sinks: slip localization in faults, damage zones, and the seismic energy budget. In: Abercrombie, R.E., McGarr, A., Di Toro, G., Kanamori, H. (Eds.), Radiated Energy and the Physics of Earthquake Faulting. American Geophysical Union Monograph, pp. 217–222.

Shipton, Z.K., Soden, A.K., Kirkpatrick, J.P., Bright, A.M., Lunn, R.J., 2006b. How thick is a fault? Fault displacement-thickness scaling revisited. In: Abercrombie, R.E., McGarr, A., Di Toro, G., Kanamori, H. (Eds.), Radiated Energy and the Physics of Earthquake Faulting. American Geophysical Union Monograph, pp. 193–198.

Sibson, R.H., 1975. Generation of pseudotachylyte by ancient seismic faulting. Geophysical Journal of the Royal Astronomical Society 43, 775–794.

Spray, J.G., 1992. A physical basis for the frictional melting of some rock forming minerals. Tectonophysics 204, 205–221.

Stipp, M., Stünitz, H., Heilbronner, R., Schmid, S., 2002. The eastern Tonale fault zone: a 'natural laboratory' for crystal plastic deformation of quartz over a temperature range from 250 to 700 °C. Journal of Structural Geology 24, 1861–1884.

Swanson, M.T., 1988. Pseudotachylyte-bearing strike-slip duplex structures in the Fort Foster Brittle Zone, S. Maine. Journal of Structural Geology 10, 813–828.

Swanson, M.T., 1992. Fault structure, wear mechanisms and rupture processes in pseudotachylyte generaton. Tectonophysics 204, 223–242.

Sibson, R.H., Toy, V.G., 2006. The habitat of fault-generated pseudotachylyte: presence vs. absence of friction-melt. In: Abercrombie, R.E., McGarr, A., Di Toro, G., Kanamori, H. (Eds.), Radiated Energy and the Physics of Earthquake Faulting. American Geophysical Union Monograph.

Zechmeister, M.S., Ferre, E.C., Cosca, M.A., Geissman, J.W., 2007. Slow and fast deformation in the Dora Maira Massif, Italian Alps: pseudotachylytes and inferences on exhumation history. Tectonophysics 29, 1114–1130.